Structural basis of action for a human ether-a-go-go-related gene 1 potassium channel activator

Matthew Perry*†, Frank B. Sachse*‡, and Michael C. Sanguinetti*†§

*Nora Eccles Harrison Cardiovascular Research and Training Institute and Departments of †Physiology and ‡Bioengineering, University of Utah, 95 South 2000 East, Salt Lake City, UT 84112

Edited by David E. Clapham, Harvard Medical School, Boston, MA, and approved July 2, 2007 (received for review April 30, 2007)

Activation of human ether-a-go-go-related gene 1 (hERG1) K^+ channels mediates cardiac action potential repolarization. Drugs that activate hERG1 channels represent a mechanism-based approach for the treatment of long QT syndrome, a disorder of cardiac repolarization associated with ventricular arrhythmia and sudden death. Here, we characterize the mechanisms of action and the molecular determinants for binding of RPR260243 [(3*R*,4*R*)-4-[3-(6-methoxy-quinolin-4-yl)-3-oxo-propyl]-1-[3-(2,3,5-trifluoro-phenyl)-prop-2-ynyl]-piperidine-3-carboxylic acid] (RPR), a recently discovered hERG1 channel activator. Channels were heterologously expressed in *Xenopus laevis* oocytes, and currents were measured by using the two-microelectrode voltage-clamp technique. RPR induced a concentration-dependent slowing in the rate of channel deactivation and enhanced current magnitude by shifting the voltage dependence of inactivation to more positive potentials. This mechanism was confirmed by demonstrating that RPR slowed the rate of deactivation, but did not increase current magnitude of inactivation-deficient mutant channels. The effects of RPR on hERG1 kinetics and magnitude could be simulated by reducing three rate constants in a Markov model of channel gating. Point mutations of specific residues located in the S4–S5 linker or cytoplasmic ends of the S5 and S6 domains greatly attenuated or ablated the effects of 3 μM RPR on deactivation (five residues), inactivation (one residue), or both gating mechanisms (four residues). These findings define a putative binding site for RPR and confirm the importance of an interaction between the S4–S5 linker and the S6 domain in electromechanical coupling of voltage-gated K^+ channels.

voltage clamp | *Xenopus* | long QT syndrome

Human ether-a-go-go-related gene 1 (hERG1) α-subunits coassemble to form channels that conduct I_{Kr} (1–3), the rapid delayed rectifier K^+ current that contributes to normal repolarization of cardiac action potentials (4). Loss-of-function mutations in hERG1 cause inherited long QT syndrome (LQTS), a disorder characterized by delayed repolarization of ventricular action potentials and prolonged QT interval of the body surface electrocardiogram (5). The acquired form of LQTS is more common and is most often caused by unintended block of hERG1 channels by a plethora of common medications (6). Inherited and acquired LQTS are associated with an increased risk of torsades de pointes, an arrhythmia that can degenerate into ventricular fibrillation and cause sudden death (7).

Current treatments for inherited LQTS include the administration of β-adrenergic receptor blockers, left cardiac sympathetic denervation, or implantation of cardiac defibrillators for the most severe cases (8). However, pharmacologic treatment is not always effective (9) and surgery or devices are expensive and require invasive procedures. Acute episodes of drug-induced LQTS are treated with magnesium sulfate administration and discontinued use of the suspect medication. Activation of hERG1 could provide an alternative and more specific treatment for acquired or inherited LQTS. Moreover, enhanced hERG1 channel activity was proposed as a novel mechanism to suppress action potential duration alternans, an electrical disorder associated with arrhythmic risk (10, 11). Several compounds were recently identified that enhance hERG1 activity and shorten cardiac action potentials. NS1643 (12, 13) and PD-118057 (14) increase current magnitude without much effect on channel kinetics, whereas RPR260243 [(3*R*,4*R*)-4-[3-(6-methoxy-quinolin-4-yl)-3-oxo-propyl]-1-[3-(2,3,5-trifluoro-phenyl)-prop-2-ynyl]-piperidine-3-carboxylic acid] (RPR) (15) primarily slows the rate of hERG1 deactivation. A detailed analysis of the mechanism of action of these drugs could facilitate the discovery of more potent and specific hERG1 activators.

Here, we show that RPR induces two distinct changes in hERG1 gating: a slowing of deactivation and a positive shift in the voltage dependence of inactivation. Functional analysis of mutant channels suggests that RPR binds to a cluster of residues located near the cytoplasmic ends of the S5 and S6 helices of the hERG1 subunit.

Results

RPR Enhances hERG1 Current Magnitude and Slows Deactivation. The effects of 3 and 30 μM RPR on hERG1 channel currents are illustrated in Fig. 1*A*. RPR caused a concentration-dependent enhancement of current magnitude, a slight slowing of activation and a pronounced slowing of tail current (I_{tail}) deactivation [Fig. 1 *A* and *B*; supporting information (SI) Fig. 6]. Kang *et al.* (15) previously reported that RPR slows the rate of hERG deactivation in CHO cells, but the increase in current magnitude by 10 μM ($\approx$15%) was less than we observed in oocytes. I_{test}, the current measured at the end of 2-s test pulses, was enhanced by RPR in a concentration- and voltage-dependent manner as seen in the *I–V* relationships (Fig. 1*C*). The voltage dependence of channel activation was determined by fitting the magnitude of I_{tail} as a function of test voltage (V_{test}) to a Boltzmann function. This relationship was not altered by RPR except at 30 μM, where a -5.2 ± 0.8 mV shift in the half-point ($V_{0.5}$) was observed (Fig. 1*D*). Thus, the increase in I_{test} is not due to an effect on channel activation.

RPR Reduces hERG1 Current Inactivation. Rapid P-type inactivation (16) reduces hERG1 current magnitude at positive potentials

Author contributions: M.P. and M.C.S. designed research; M.P. performed research; M.P. and F.B.S. analyzed data; and M.P. and M.C.S. wrote the paper.

The authors declare no conflict of interest.

This article is a PNAS Direct Submission.

Abbreviations: hERG1, human ether-a-go-go-related gene potassium channel type 1a; LQTS, long QT syndrome; RPR, [(3*R*,4*R*)-4-[3-(6-methoxy-quinolin-4-yl)-3-oxo-propyl]-1-[3-(2,3,5-trifluoro-phenyl)-prop-2-ynyl]-piperidine-3-carboxylic acid].

§To whom correspondence should be addressed. E-mail: sanguinetti@cvrti.utah.edu.

This article contains supporting information online at www.pnas.org/cgi/content/full/0703934104/DC1.

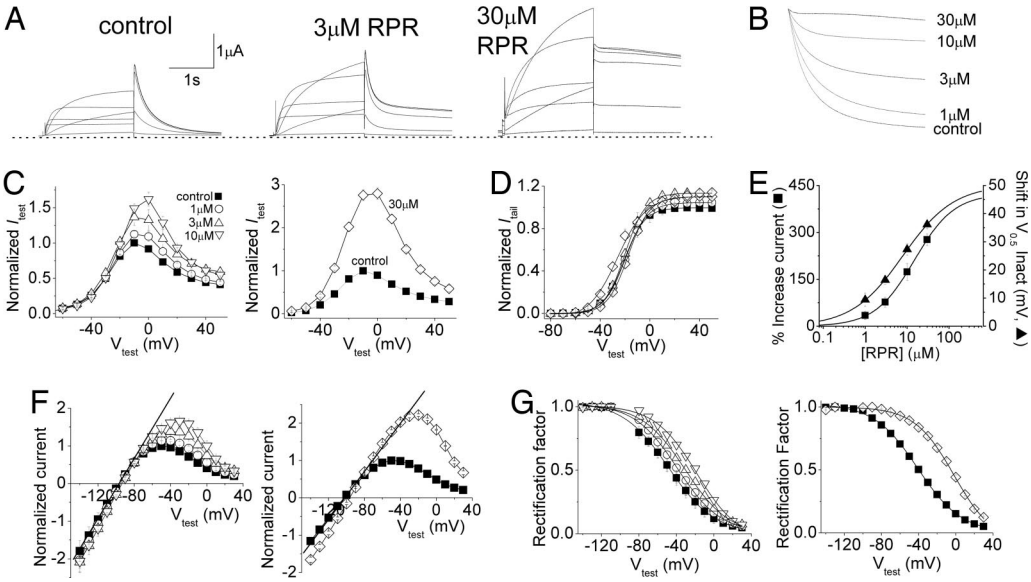

Fig. 1. Effects of RPR on hERG1 channel current recorded in *Xenopus* oocytes. (*A*) RPR increases the magnitude and slows deactivation of hERG1 current. The currents shown were elicited with 2-s pulses from −50 to +50 mV in 20-mV increments. Tail currents (I_{tail}) were measured at −70 mV. (*B*) RPR slows hERG1 deactivation. Superimposed tail currents recorded at −70 mV were normalized relative to their peak value before (control) and after addition of the indicated concentration of RPR. (*C*) Effects of RPR on *I–V* relationships for 1, 3, and 10 μM RPR (*Left*) or 30 μM RPR (*Right*). (*D*) Effects of RPR on voltage dependence for activation. I_{tail} were normalized relative to peak value under control conditions. (*E*) [RPR]-dependent changes in current magnitude and voltage dependence of inactivation. The increase in peak outward $I_{tail\text{-}FA}$ at 0 mV (■) was measured from the fully activated *I–V* relationship (EC_{50} = 15 ± 2.6 μM; Hill coefficient, 0.91). The shift in $V_{0.5}$ for inactivation (▲) was calculated from plots shown in *G* (EC_{50} = 8.0 ± 1.5 μM; Hill coefficient, 0.71). (*F*) Fully activated *I–V* relationships, normalized relative to peak outward $I_{tail\text{-}FA}$ in control. (*G*) Voltage dependence of hERG1 inactivation determined from rectification of the fully activated *I–V* relationship. Concentration of RPR in *C*, *D*, *F*, and *G* are as follows: control (■); 1 μM (○), 3 μM (△), 10 μM (▽), and 30 μM (◇) RPR.

and causes inward rectification of the fully activated *I–V* relationship (Fig. 1*F*), as determined by measuring peak tail currents ($I_{tail\text{-}FA}$) on repolarization to a variable V_{test} after a 2-s prepulse to +40 mV (SI Fig. 6*A*). At 30 μM, RPR induced a ≈3-fold increase of $I_{tail\text{-}FA}$ at 0 mV, but only a small increase in maximal conductance, estimated from the linear fit of $I_{tail\text{-}FA}$ measured at potentials between −140 and −80 mV (Fig. 1*F*). In guinea pig myocytes, RPR enhanced I_{Kr} tail currents measured at −50 mV by 70% at 10 μM and 106% at 30 μM (15), consistent with our results in oocytes at a similar voltage (Fig. 1*F*).

The deviation of the fully activated *I–V* relationship from linearity was used to estimate the voltage dependence for hERG1 inactivation (Fig. 1*G*). RPR shifted the $V_{0.5}$ for this relationship (from −48.8 ± 2.4 mV under control conditions) by +10.2 ± 2.4 mV at 1 μM (n = 8), +17.2 ± 1.6 mV at 3 μM (n = 13), +28 ± 2 mV at 10 μM (n = 10), and +36.9 ± 1.3 mV at 30 μM (n = 4). The effects of RPR on current amplitude and $V_{0.5}$ for inactivation was reversible on washout of the drug, and unrelated to initial current magnitude or extracellular K^+ accumulation (data not shown). The EC_{50} for the shift in $V_{0.5}$ was 8.0 μM (Fig. 1*E*). RPR enhanced $I_{tail\text{-}FA}$ magnitude measured at 0 mV with an EC_{50} of 15 μM (Fig. 1*E*). A Hill coefficient near 1 for these relationships is consistent with the requirement for only one RPR molecule/channel; however, further study is required to resolve the stoichiometry of the drug–channel interaction. In summary, the [RPR]-dependent increase in hERG1 current was highly correlated with a positive shift in the voltage dependence of inactivation.

Markov Model of Altered hERG1 Channel Gating by RPR. A two-compartment Markov model was used to simulate the concentration-dependent effects of RPR (Fig. 2*A*). Drug-bound channels were reconstructed by reducing the rate coefficients for the transitions between open and closed states ($O_d \leftrightarrow C_{d,2}$) and the transition from the open to the inactivated state ($O_d \rightarrow I_d$). This simple model can account for the [RPR]-dependent increase in current magnitude (Fig. 2*B*), slowed deactivation (Fig. 2*C*), altered *I–V* relationship (Fig. 2*D*), lack of effect on the voltage dependence of activation (Fig. 2*E*), rightward shift in the voltage dependence of inactivation (Fig. 2*F*), and [RPR]-dependent increase in $I_{tail\text{-}FA}$ (Fig. 2*G*).

Scanning Mutagenesis Identifies a Putative Binding Site for RPR. Several compounds that activate KCNQ channels have been described, including retigabine (17, 18), R-L3 (19), and zinc pyrithione (20). Retigabine and R-L3 enhance the magnitude and slow the deactivation of KCNQ2–5 and KCNQ1 channel currents, respectively, and both compounds interact with residues in the S5 and S6 domains of the KCNQ subunits (17–19). By analogy, we hypothesized that RPR might bind to a similar region in hERG1. Therefore, we mutated individual residues located within the S4–S5 linker, S5 and S6 helices of hERG1 and determined the effect of 3 μM RPR on these mutant channels. Most of the 40 residues examined were mutated to Ala (or Ala to Val). For a few residues, as noted in *Materials and Methods*, other substitutions were made to enhance levels of channel expression. Seven of the mutant channels were nonfunctional, or expressed very poorly, and were not studied further. We determined the effects of 3 μM RPR on the remaining 33 mutant channels. Four mutations (L553A, F557L, N658A, and V659A) prevented the slowing of deactivation (Fig. 3*A*, red bars) and reduced or eliminated the shift in $V_{0.5}$ for inactivation (Fig. 3*B*, red bars) by 3 μM RPR. In contrast, mutation of five other residues (I662, L666, Y667, V549, and L550) attenuated the effects on deactivation (Fig. 3*A*, blue bars), but not inactivation (Fig. 3*B*, blue bars). Finally, RPR slowed deactivation, but did not alter inactivation of Y652A channels (Fig. 3 *A* and *B*, green bars). Similar to WT hERG1, the drug-induced increase in $I_{tail\text{-}FA}$ at 0 mV for mutant channels was highly correlated with the shift in the $V_{0.5}$ for inactivation (Fig. 3*C*). Examples of mutant

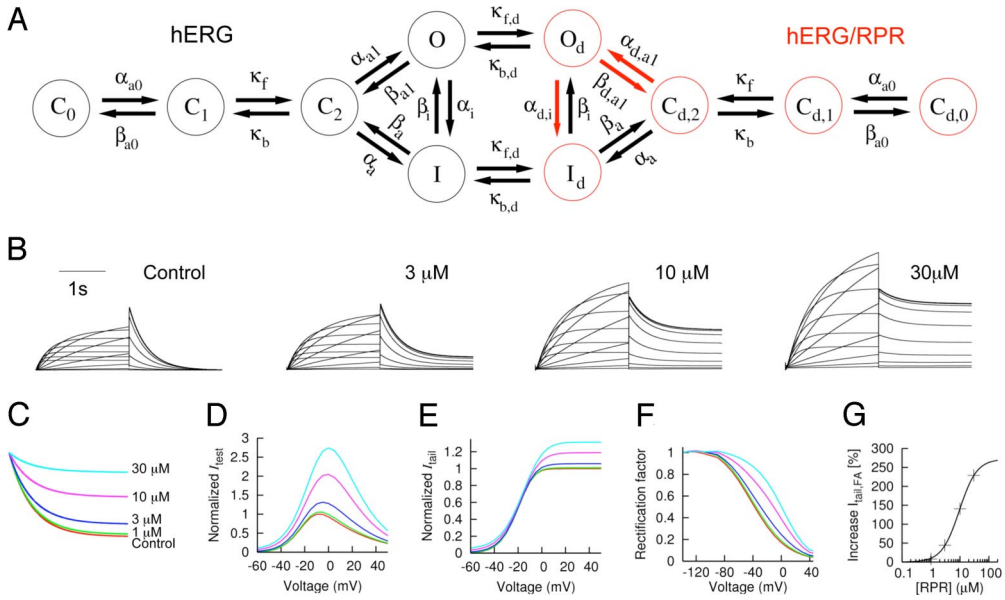

Fig. 2. Model of hERG1 channel-gating as modified by RPR. (*A*) Two-compartment Markov model. The model assumes two populations of channels, with and without RPR bound to hERG1. Drug-bound channels were reconstructed by reducing the rate coefficients of the transition $O_d \rightarrow C_{d,2}$ by 99.8% (slowed deactivation), $C_{d,2} \rightarrow O_d$ by 67% (slowed activation), and $O_d \rightarrow I_d$ by 87% (reduced inactivation) in comparison with the rate coefficients of WT hERG1. Transitions between the compartments ($O \leftrightarrow O_d$ and $I \leftrightarrow I_d$) were described with an equilibrium dissociation constant $K_d = K_{b,d}/K_{f,d} = 5 \times 10^{-8}$ M[1.7]. Details of the model, including rate constants and initial values for each state, are provided in SI Table 1. (*B*) Simulated hERG1 currents in response to voltage-clamp pulses from −60 to +50 mV, applied in 10-mV increments. (*C*) Simulated effects of RPR on hERG1 tail currents measured at −70 mV. (*D*) Plot of normalized I_{test} vs. V_{test} for 2-s pulses. (*E*) Plot of normalized I_{tail} vs. V_{test}. (*F*) Plot of rectification factor vs. V_{test}. Colors in *D–F* correspond to the same [RPR] as shown in *C*. (*G*) [RPR]-dependent increase in $I_{tail\text{-}FA}$ at 0 mV. A fit to the Hill equation yielded a Hill coefficient of 1.4 and a half-saturation concentration [$RPR_{50\%}$] of 9.4 μM.

channel currents from each category of RPR response are presented in SI Fig. 7.

Mutation of key residues reduced, but did not eliminate the effects of RPR on channel gating. At a high concentration (30 μM), RPR slightly slowed deactivation and shifted the $V_{0.5}$ for inactivation by <10 mV for F557L hERG or L666A hERG channels, equivalent to effects achieved with 1 μM RPR on WT channels (SI Fig. 8). In addition, 30 μM RPR decreased the amplitude of fully activated L666A hERG current (SI Fig. 8), suggesting that high concentrations of RPR can also block the channel.

The important residues identified by mutation analysis are highlighted in a homology model of the hERG1 subunit (Fig. 4) based on the crystal structure of Kv1.2 in the open state (21). The sequence of the S4–S5 linker and S5 domains of hERG1 do not align well with Kv1.2. In addition, hERG1 lacks the PVP motif in the S6 domain, a crucial structural determinant of the activation gate of Kv1.2. In view of these limitations, the mapping of residues in the S4–S5 linker and S5 domains is problematic. Nonetheless, by using the most reasonable alignment predicted by Insight II, the key residues identified by our scanning mutagenesis results constitute two adjacent clusters near the intersection of the cytoplasmic ends of the S5 and S6 domains. One group of residues (cluster 1, colored red) corresponds to mutations that attenuated all effects of RPR; the other group of residues (cluster 2, colored blue) corresponds to mutations that only eliminated the effect of RPR on deactivation.

Paired Point Mutations Eliminate Effects of RPR on Inactivation and Deactivation. S631A hERG1 channels have impaired inactivation gating (22). As expected for an inactivation-deficient channel, RPR (3 μM) slowed the rate of deactivation, but did not alter the magnitude of S631A channel currents (Fig. 5*A*). In contrast, RPR increased current magnitude (Fig. 5*B*), but did not alter deactivation (Fig. 5*B Inset*) of L666A hERG1 channels. Channels harboring both mutations (S631A/L666A) were completely insensitive to 3 μM RPR (Fig. 5*C*). Similar results were obtained when L666A was combined with another point mutation (S620T) that disrupts inactivation (Fig. 5*D* and SI Fig. 9*B*). The lack of effect of RPR was observed over a wide range of test potentials (Fig. 5*E*). Moreover, other mutations that impair inactivation (G628C/S631C or N588K) also prevented the increase in current magnitude by RPR (SI Fig. 9). These data confirm that the enhancement of hERG1 current by RPR is mediated by altered inactivation gating that can be mechanistically differentiated from the drug-induced slowing of deactivation.

Discussion

RPR modified hERG1 channel gating by two distinct mechanisms. First, RPR slowed the rate of deactivation with little or no effect on the voltage dependence of channel activation. Drug-induced slowing of deactivation can be modeled by a reduction in a single rate constant that defines the open to closed state transition ($O_d \rightarrow C_{d,2}$). Second, the increased magnitude of I_{test} was caused by a positive shift in the voltage dependence of P-type inactivation. As predicted for this proposed mechanism, RPR did not increase I_{test} of inactivation-deficient mutant hERG1 channels. The effect on inactivation can be modeled by a decrease in the rate constant for the open to inactivated state transition ($O_d \rightarrow I_d$).

A putative binding site for RPR was defined by using site-directed mutagenesis. Mutation of four residues (cluster 1) attenuated all of the effects of RPR. Based on our homology model of hERG1, cluster 1 residues (colored red in Fig. 4) are located in S5 (L553, F557) and an adjacent region of S6 (N658, V659). Presumably, when RPR interacts with these residues, it affects channel rearrangements associated with both deactivation and inactivation gating. Deactivation of K^+ channels is mediated by bending of the S6 helices in all four subunits toward the central axis of the pore (23), a gating process that is slowed when RPR is bound to a hERG1

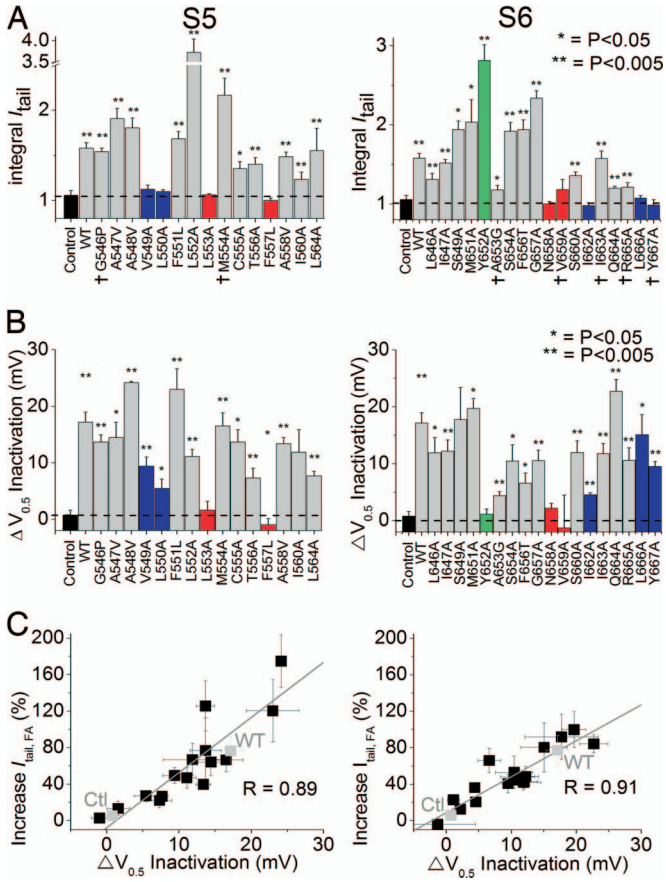

Fig. 3. Effect of RPR on WT and mutant hERG1 channels. (*A*) Effect of 3 μM RPR on deactivation of WT and mutant hERG1 channels quantified by $\int I_{tail\text{-}drug}/\int I_{tail\text{-}control}$ (integral I_{tail}) at −70 mV (†, or at −110 mV for very slow deactivating mutant channels). (*B*) Shift in $V_{0.5}$ for inactivation of WT and mutant channels by 3 μM RPR. Mutations that reduced both gating effects of RPR are colored red. Mutations that prevented the slowing of deactivation, but not the shift of inactivation, are colored blue. Mutation of Y652 (colored green) to Ala prevented the increase in current by RPR but not the slowing of deactivation. Left graphs show mutations in S4–S5 linker (G546–L552) and S5; right graphs show S6 mutations. Some mutant channels did not express sufficient current to allow quantitative study, including L559, H562, and W563 (S5) and L650 and I655 (S6). (*C*) Plot of the shift in $V_{0.5}$ for inactivation and percentage increase of $I_{tail\text{-}FA}$ at 0 mV in the presence of 3 μM RPR for WT and all mutant hERG1 channels described in this study. The line represents linear regression (R = 0.89 for S5 and 0.91 for S6 residues).

subunit. P-type inactivation of K^+ channels probably involves subtle movements of the selectivity filter (24), a structure that is distant from the proposed binding site for the drug. Presumably, RPR affects inactivation gating by an allosteric effect, perhaps by indirectly altering a voltage-dependent conformational change in the S5–P linker, a structure proposed to be involved in hERG1 inactivation (25).

Point mutations of five other amino acids (cluster 2) prevented the slowing of deactivation by RPR, but not the drug-induced increase in current magnitude. Cluster 2 residues (colored blue in Fig. 4) are located in adjacent regions of the S4–S5 linker (V549, L550) and cytoplasmic end of S6 (I662, L666, Y667). The concerted movements of S4, S4–S5 linker, and S6 domains mediate electromechanical coupling (21), the voltage-dependent opening and closing of K^+ channels, including hERG1 (26–28). Interactions between multiple residues in cluster 2 might be required to mediate the slowing of deactivation when RPR is bound to the residues of cluster 1. Alternatively, cluster 2 residues may define a second binding

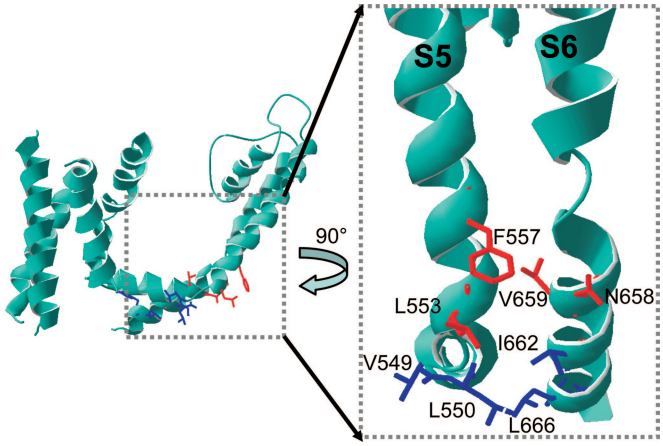

Fig. 4. Homology model for a single hERG1 subunit, highlighting the residues identified by Ala mutagenesis as important for interaction with RPR. The boxed region in *Left* is shown in an expanded, rotated, and tilted view at *Right*. Residues identified by mutagenesis as important for RPR activity are labeled in *Right*. The color of the highlighted residue side chains correspond to the coding described in Fig. 3. Sequence alignment between hERG1 and Kv1.2 used for this model is shown in SI Fig. 10.

site that, when bound by drug, does not affect channel deactivation. Regardless of the precise mechanism, our findings with RPR reinforce the importance of the interaction between the S4–S5 linker and S6 for normal gating of hERG1 (26, 28).

The putative binding site for RPR is distinct from the site described for drugs that block hERG1 channels. The binding site for structurally diverse blockers was previously localized to specific residues in S6 and the base of the pore helix that face toward the central cavity (29). F656 and Y652 in S6 are the most important residues for binding of blockers. F656T hERG1 channels are relatively insensitive to hERG1 blockers (30), but responded normally to RPR (SI Fig. 7*A*). In contrast, RPR greatly slowed the deactivation of Y652A hERG1, but did not increase current magnitude or affect the voltage dependence of inactivation (SI Fig. 7*C*). It is unlikely that Y652 contributes to the RPR binding site because it is located on the opposite side of S6 from the other critical residues identified by mutagenesis. Instead, Y652 may be critical for allosteric coupling between RPR binding and altered P-type inactivation.

Another hERG1 activator, NS1643, also enhances hERG1 current by causing a shift in the voltage dependency of inactivation (12) and the agonist effect of PD-118057 was greater at more positive potentials (14), suggesting a similar mechanism of action. However, in contrast to RPR, PD-118057 did not appreciably affect hERG1 deactivation, suggesting that these drugs bind to distinct sites.

In summary, RPR alters deactivation and inactivation gating of hERG1 channels by interaction with a cluster of residues located near the cytoplasmic ends of the S5 and S6 domains of a single channel subunit. These residues define a putative binding site for RPR that is distinct from the binding site for channel blockers. Direct interference of electromechanical coupling between the S4–S5 linker and S6 by RPR mediates slowed deactivation, whereas inactivation likely is altered by an allosteric mechanism. Enhancement of hERG activity by reduced inactivation alone or combined with slower deactivation shortens action potential duration in cardiac myocytes (13, 15). It remains to be determined whether a single or combined mechanism of drug action will provide a safe and effective treatment for acquired or inherited LQTS.

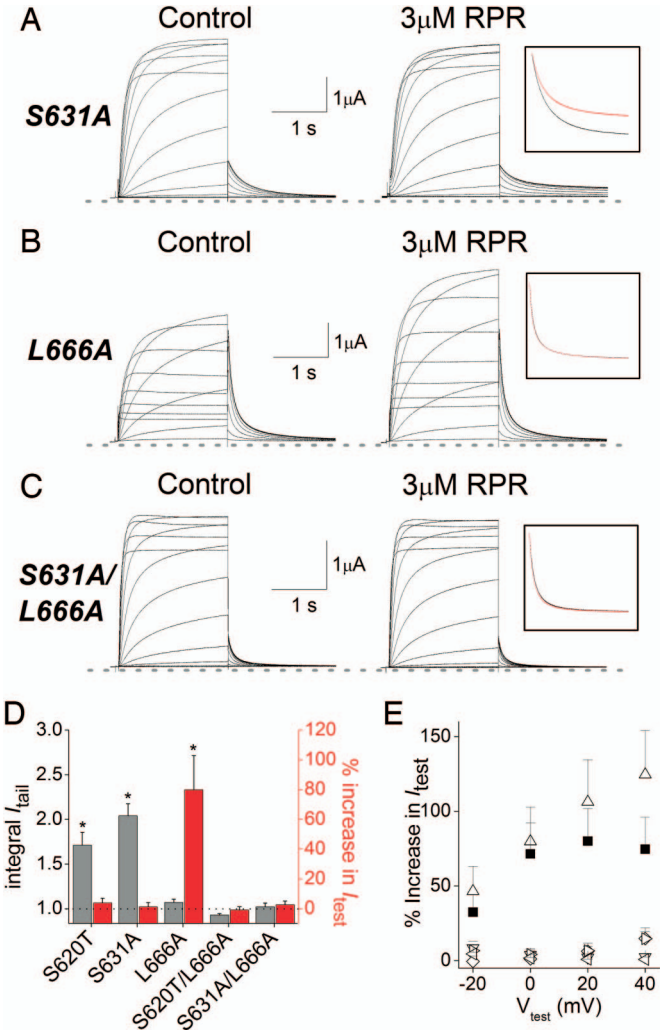

Fig. 5. Inactivation-deficient and L666A hERG1 channels are less sensitive to RPR. (*A*) RPR slows deactivation but does not increase current magnitude of S631A hERG1. (*Inset*) Superimposed and normalized tail current traces for control and after 3 μM RPR. (*B*) RPR increases the magnitude of L666A hERG1 currents but has no effect on the rate of deactivation (*Inset*). (*C*) Channels with double mutation (S631A/L666A) are insensitive to 3 μM RPR. In *A–C*, currents were recorded at test potentials of −60 to +50 mV, applied in 10-mV increments and tail currents were measured at −70 mV. (*D*) Normalized $\int I_{tail}$ and percentage increase in I_{test} at 0 mV for indicated mutant hERG1 channels. (*E*) Percentage increase in I_{test} at different voltages for WT (■), L666A (△), S631A (◇), S620T (▽), N588K (◁), and G628C/S631C (▷) hERG1 channels ($n \geq 4$). S620T (36), N588K (37), and G628C/S631C (38) are mutations that eliminate or disrupt hERG1 inactivation.

Materials and Methods

Channel Mutagenesis and Expression in *Xenopus* Oocytes. *HERG1* (*KCNH2*, isoform 1a) was cloned into the pSP64 oocyte expression vector and 40 mutations were introduced by site-directed mutagenesis by using QuickChange (Stratagene, La Jolla, CA). Residues 546–564 and 646–667 were mutated to Ala (or to Val for Ala residues), with the exception of five residues. Mutation to Ala (or Val) of 12 residues resulted in poorly expressing or nonfunctional channels. Seven of these mutations (L559A, A561V, H562A, W563A, G648A, L650A, I655A) were not further studied. To enhance expression, alternate substitutions were made for F551 and F557 (mutated to Leu), G546 (mutated to Pro), A653 (mutated to Gly), and F656 (mutated to Thr). A661 was not mutated. cRNA was prepared by *in vitro* transcription with SP6 Cap-Scribe (Roche, Indianapolis, IN) after linearization of the vector plasmid with EcoR1. I662A hERG (provided by J. Mitcheson, University of Leicester, Leicester, U.K.) was subcloned into pcDNA3 and *in vitro* transcribed with T7 Cap-Scribe (Roche). The isolation, culture, and injection of oocytes with cRNA were performed as described (31).

Voltage Clamp. Currents were recorded from oocytes 1–5 days after cRNA injection by using the two-electrode voltage-clamp technique as described (32). Oocytes were voltage clamped to a holding potential of −90 mV, before applying a depolarizing pulse to 0 mV for 5 s to activate test currents (I_{test}). A repolarization to −70 mV for 800 ms was used to activate tail currents (I_{tail}). Continuous pulses were applied every 8 s (or 30 s after RPR) until steady-state levels of current were achieved. Standard *I–V* relationships were evaluated by eliciting 2-s depolarizations (from a holding potential of −90 mV) to a range of test potentials between −80 and +50 mV. Each test pulse was followed by a 2-s repolarizing pulse to −70 mV (or −110 mV for slowly deactivating mutant channels) to determine I_{tail} amplitude, voltage dependence of I_{test} activation, and the rate of I_{tail} deactivation, quantified as $\int I_{tail\text{-}drug}/\int I_{tail\text{-}control}$. Both the steady-state and voltage dependence protocols were then repeated 10–15 min after the addition of RPR to the bathing solution. In the absence of drug, the increase in I_{test} for WT hERG1 during an equivalent 10-min period after switching between control solutions in the absence and presence of 0.03% DMSO was 1.5 ± 6% ($n = 5$).

The fully activated *I–V* relationship was determined by applying 2-s prepulses to +40 mV, followed by measuring tail currents ($I_{tail\text{-}FA}$) on repolarization to a variable V_{test}. The extent of inward rectification of hERG1 was quantified by the deviation of $I_{tail\text{-}FA}$ values from that predicted by linear extrapolation of $I_{tail\text{-}FA}$ measured at V_{test} of −140 to −110 mV to more positive potentials. The deviation of the *I–V* relationships from linearity was corrected by the driving force for K^+ ($V_{test} - E_{rev}$) to obtain a rectification factor for each value of V_{test}. Finally, the plot of rectification factor vs. V_{test} was fitted with a Boltzmann function to obtain the voltage dependence for hERG1 inactivation. Each oocyte was treated with a single concentration of RPR.

Digitized data were analyzed off-line with pCLAMP8 (Molecular Devices, Sunnyvale, CA) and ORIGIN 7.5 (OriginLab, Northhampton, MA) software.

Solutions and Drugs. The extracellular solution contained 96 mM NaCl, 2 mM KCl, 1 mM $CaCl_2$, 5 mM Hepes, and 2 mM $MgCl_2$, pH adjusted to 7.6 with NaOH. RPR was kindly donated by David Rampe (Sanofi-Aventis Pharmaceuticals, Bridgewater, NJ). Drug solutions were prepared daily by dilution of a 10 mM DMSO stock solution.

Modeling. A Markov model of hERG1 channels was developed to simulate the effects of increasing concentrations of RPR on I_{Kr}. The model includes two compartments representing populations of hERG1 channels in normal and drug-bound states (Fig. 2*A*). Each compartment is based on a previously described model of hERG1 channels at 37°C (33, 34). The rate constants for each transition were of the standard format: $\alpha = \alpha_0 \exp[z_\alpha V_m/(RT/F)]$ and $\beta = \beta_0 \exp[-z_\beta V_m/(RT/F)]$. The original rate coefficients were adjusted with a temperature coefficient $Q_{10} = 3.3$ for reconstruction of currents at room temperature. The drug-bound compartment was parameterized by using the normalized I_{test} and I_{tail} (Fig. 1 *C* and *D*) in a numerical optimization procedure. The parameterization affected rate coefficients describing the transition from O_d to I_d and between O_d and $C_{d,2}$. Transitions between the compartments represent the binding and washout of RPR. The transitions were defined for the O and I states ($O \leftrightarrow O_d$ and

$I \leftrightarrow I_d$) with the rate coefficients $K_{f,d}$ and $K_{b,d}$, which were determined by least-square fit to deactivation ratios of I_{tail} at 0 mV for the different concentrations of RPR. Simulations were carried out with the Euler method for numerical solution of ordinary differential equations (35). A time step (Δt) of 25 μs was chosen. All calculations were performed in double precision.

The Kv1.2 structure and sequence (21) was used as the template for a hERG homology model created with Insight II Modeler (version 8.2; Accelrys, San Diego, CA).

We thank John Mitcheson and David Fernandez for helpful comments. This work was supported by National Institutes of Health/National Heart, Lung, and Blood Institute Grant HL055236.

1. Jones EM, Roti Roti EC, Wang J, Delfosse SA, Robertson GA (2004) *J Biol Chem* 279:44690–44694.
2. Sanguinetti MC, Jiang C, Curran ME, Keating MT (1995) *Cell* 81:299–307.
3. Trudeau M, Warmke JW, Ganetzky B, Robertson GA (1995) *Science* 269:92–95.
4. Sanguinetti MC, Jurkiewicz NK (1990) *J Gen Physiol* 96:195–215.
5. Curran ME, Splawski I, Timothy KW, Vincent GM, Green ED, Keating MT (1995) *Cell* 80:795–803.
6. Sanguinetti MC, Mitcheson JS (2005) *Trends Pharmacol Sci* 26:119–124.
7. Keating MT, Sanguinetti MC (2001) *Cell* 104:569–580.
8. Schwartz PJ (2006) *J Intern Med* 259:39–47.
9. Moss AJ, Zareba W, Hall WJ, Schwartz PJ, Crampton RS, Benhorin J, Vincent GM, Locati EH, Priori SG, Napolitano C, *et al.* (2000) *Circulation* 101:616–623.
10. Hua F, Gilmour RF, Jr (2004) *Circ Res* 94:810–819.
11. Hua F, Johns DC, Gilmour RF, Jr (2004) *Am J Physiol* 286:H2342–H2351.
12. Casis O, Olesen SP, Sanguinetti MC (2006) *Mol Pharmacol* 69:658–665.
13. Hansen RS, Diness TG, Christ T, Demnitz J, Ravens U, Olesen S-P, Grunnet M (2005) *Mol Pharmacol* 69:266–277.
14. Zhou J, Augelli-Szafran CE, Bradley JA, Chen X, Koci BJ, Volberg WA, Sun Z, Cordes JS (2005) *Mol Pharmacol* 68:876–884.
15. Kang J, Chen XL, Wang H, Ji J, Cheng H, Incardona J, Reynolds W, Viviani F, Tabart M, Rampe D (2005) *Mol Pharmacol* 67:827–836.
16. De Biasi M, Hartmann HA, Drewe JA, Taglialatela M, Brown AM, Kirsch G (1993) *Pflügers Arch* 422:354–363.
17. Schenzer A, Friedrich T, Pusch M, Saftig P, Jentsch TJ, Grotzinger J, Schwake M (2005) *J Neurosci* 25:5051–5060.
18. Wuttke TV, Seebohm G, Bail S, Maljevic S, Lerche H (2005) *Mol Pharmacol* 67:1009–1017.
19. Seebohm G, Pusch M, Chen J, Sanguinetti MC (2003) *Circ Res* 93:941–947.
20. Xiong Q, Sun H, Li M (2007) *Nat Chem Biol* 3:287–296.
21. Long SB, Campbell EB, Mackinnon R (2005) *Science* 309:897–903.
22. Zou A, Xu QP, Sanguinetti MC (1998) *J Physiol (London)* 509:129–138.
23. Webster SM, Del Camino D, Dekker JP, Yellen G (2004) *Nature* 428:864–868.
24. Loots E, Isacoff EY (1998) *J Gen Physiol* 112:377–389.
25. Liu J, Zhang M, Jiang M, Tseng GN (2002) *J Gen Physiol* 120:723–737.
26. Ferrer T, Rupp J, Piper DR, Tristani-Firouzi M (2006) *J Biol Chem* 281:12858–12864.
27. Sanguinetti MC, Xu QP (1999) *J Physiol (London)* 514:667–675.
28. Tristani-Firouzi M, Chen J, Sanguinetti MC (2002) *J Biol Chem* 277:18994–19000.
29. Mitcheson JS, Chen J, Lin M, Culberson C, Sanguinetti MC (2000) *Proc Natl Acad Sci USA* 97:12329–12333.
30. Fernandez D, Ghanta A, Kauffman GW, Sanguinetti MC (2004) *J Biol Chem* 279:10120–10127.
31. Shih TM, Smith RD, Toro L, Goldin AL (1998) *Methods Enzymol* 293:529–556.
32. Stühmer W (1992) *Methods Enzymol* 207:319–339.
33. Iyer V, Mazhari R, Winslow RL (2004) *Biophys J* 87:1507–1525.
34. Lu Y, Mahaut-Smith MP, Varghese A, Huang CL, Kemp PR, Vandenberg JI (2001) *J Physiol (London)* 537:843–851.
35. Press WH, Teukolsky SA, Vetterling WT, Flannery BP (1992) *Numerical Recipes in C* (Cambridge Univ Press, Cambridge, UK).
36. Ficker E, Jarolimek W, Kiehn J, Baumann A, Brown AM (1998) *Circ Res* 82:386–395.
37. Brugada R, Hong K, Dumaine R, Cordeiro J, Gaita F, Borggrefe M, Menendez TM, Brugada J, Pollevick GD, Wolpert C, *et al.* (2004) *Circulation* 109:30–35.
38. Smith PL, Baukrowitz T, Yellen G (1996) *Nature* 379:833–836.